Stark broadening and shift of the first two Paschen lines of hydrogen

A. Döhrn and P. Nowack
Institut für Experimentalphysik, Universität Kiel, Olshausenstrasse 40, D 24098 Kiel, Germany

A. Könies and S. Günter
Fachbereich Physik, Universität Rostock, Universitätsplatz 1, D 18051 Rostock, Germany

V. Helbig
Institut für Experimentalphysik, Universität Kiel, Olshausenstrasse 40, D 24098 Kiel, Germany

(Received 20 November 1995)

The broadening and shift of the first two lines of the Paschen series of hydrogen have been investigated both experimentally and theoretically. The application of an earlier developed Green's-function approach predicts a nonlinear behavior of the shift of the Paschen α line that is confirmed by the observations. The experiments have been carried out applying a wall-stabilized arc running in neon or argon seeded with hydrogen. The electron density range covered by the experiments is 0.5×10^{16} cm^{-3} to 25×10^{16} cm^{-3}.

PACS number(s): 52.70.Kz, 32.70.Jz

I. INTRODUCTION

The exploitation of the Stark-effect broadening of the hydrogen lines has proven to be a valuable tool in plasma diagnostics. Given that the broadening parameters are known with high accuracy the electron density can easily be determined in a wide density range using, e.g., the Balmer α and β lines [1,2]. Though hydrogen is the simplest atomic system, a completely satisfying theory for the plasma broadening has not been formulated yet. Thus the broadening parameters necessary for the plasma diagnostics are usually taken from experimental investigations. However, the study of the Stark-effect broadening has been mainly focused on the first two Balmer lines, while only a few experimental investigations of the lines of the Lyman or Paschen series have been reported, because the experimental access to these lines is more challenging. The experimental data of the broadening of P_α and P_β are therefore scarce, and no publication giving results for the shift of these lines is known. The present work deals with the Stark effect of the first two lines of the Paschen series using both an experimental and a theoretical approach.

As the upper levels of the Paschen lines are split into more components than the levels of the Balmer or the Lyman lines, a calculation of the Stark effect is not as simple as it is in the case of the lower series members. But on the other hand many-particle effects, such as a possible nonlinear shift of the spectral lines, become visible at an earlier stage, i.e., at lower electron densities. Therefore an investigation of the Paschen series promises a better understanding of the Stark broadening of hydrogen.

II. THEORY

An earlier developed Green's-function approach to the optical properties of dense plasmas [3–6] has been applied here to calculate the asymmetric and shifted profiles of the first two Paschen lines. This approach allows a fully quantum mechanical treatment of the perturbing electrons. The influence of the dynamic plasma ions has been described within the well-known model microfield method [7–9]

$$I(\Delta\omega)=\frac{1}{\pi}\,\mathrm{Im}\sum_{i,f,i',f'} I_{i,f}^{i'f'}(\Delta\omega)\langle i|\langle f|U(\Delta\omega)|f'\rangle|i'\rangle, \tag{1}$$

where the frequency dependent intensity includes the corresponding transition matrix elements as well as the trivial asymmetry. The time development operator $U(\Delta\omega)$ will be determined applying the well-known ''kangaroo'' process [8,9]. Therefore, the time development operator for a constant ionic microfield E

$$U(\Delta\omega|E)=[\Delta\omega-\mathrm{Re}\{\Sigma_i-\Sigma_f\}+i\Omega(E)+i\,\mathrm{Im}\{\Sigma_i+\Sigma_f\}+i\Gamma^{\nu}]^{-1} \tag{2}$$

is needed. $\Omega(E)$ is the jumping frequency of the ionic microfield strength which ensures the correct field correlation function of the stochastic process [10]. The self-energy Σ describes the influence of the surrounding plasma on the radiator. It contains the electronic as well as the (static) ionic contributions.

The electronic contributions to the self-energy within a second order Born approximation are given by

$$\langle n|\Sigma^{\mathrm{el}}(E_n)|n\rangle=-\frac{1}{e^2}\int\frac{d\vec{q}}{(2\pi)^3}V(q)\sum_{\alpha}|M_{n\alpha}^{(0)}(\vec{q})|^2\times\int_{-\infty}^{\infty}\frac{d\omega}{\pi}[1+n_B(\omega)]\frac{\mathrm{Im}\varepsilon^{-1}(\vec{q},\omega+i0)}{E_n-E_\alpha-(\omega+i0)}. \tag{3}$$

Of course within this approximation the electronic contributions to the self-energy are overestimated. Therefore a partial summation of the corresponding three-particle T matrix describing the interaction between the radiator and a perturbing electron as outlined in [6] has been applied to choose the upper limit for the transition momentum q. In Eq. (3) $V(q)$ is the Coulomb potential $V(q)=e^2/\epsilon_0 q^2$, $n_B(\omega)$ denotes the

Bose function. For the transition matrix elements $M_{n\alpha}^{(0)}(\vec{q})$ an expansion into the spherical wave functions has been applied as given in [5].

The inverse dielectric function $\varepsilon^{-1}(\vec{q},\omega)$ contains many-particle effects. Usually, calculating hydrogen spectral lines, instead of the full expression

$$\mathrm{Im}\varepsilon^{-1}(\vec{q},\omega)=-\frac{\mathrm{Im}\varepsilon(\vec{q},\omega)}{[\mathrm{Re}\varepsilon(\vec{q},\omega)]^2+[\mathrm{Im}\varepsilon(\vec{q},\omega)]^2}, \quad (4)$$

various approximations have been applied. In order to calculate the linewidth which follows from virtual transitions between states of the same principal quantum number, a static Debye screening may be taken

$$\mathrm{Im}\varepsilon^{-1}(\vec{q},\omega)\approx-\frac{\mathrm{Im}\varepsilon(\vec{q},\omega)}{\left(1+\frac{\kappa_D^2}{q^2}\right)^2}, \quad (5)$$

where κ_D is the inverse Debye radius

$$\kappa_D^{-1}=[(e^2n_e)/(\epsilon_0k_BT)]^{-1/2}=r_D. \quad (6)$$

In determining line shifts, however, a binary collision approximation

$$\mathrm{Im}\varepsilon^{-1}(\vec{q},\omega)\approx-\mathrm{Im}\varepsilon(\vec{q},\omega) \quad (7)$$

has often been applied. Keeping in mind that the main contributions to the shift result from virtual transitions between states of different principal quantum numbers ($\Delta n\neq 0$), according to Eq. (3), this approximation is valid only if the energy difference between this states $\omega_{n\alpha}=E_n-E_\alpha$ is much larger than the electron plasma frequency

$$\omega_{\mathrm{pl}}=\left[\frac{(n_ee^2)}{(\epsilon_0m_e)}\right]^{1/2}. \quad (8)$$

Applying a binary collision approximation to the line shift, results in a linear dependence of the shift on the electron density.

The ionic contributions to the self-energy contain the linear and the quadratic Stark effect as well as the interaction between the radiator and the inhomogeneities of the ionic microfield. The ion quadrupole effect has been included applying the theory given by Halenka [11] who generalized Sholin's formulas [12,13] in order to account for the screening of the ionic microfields by the plasma electrons as well as for pair correlations between the ions in the Baranger-Mozer limit.

Applying the developed theory it is possible to calculate the shifted and asymmetric line profiles. The theoretical line shift given here is the maximum shift of the profile as it is in the experiment.

III. EXPERIMENTAL SETUP

The spectra of the hydrogen Paschen lines were obtained from the plasma of a wall-stabilized arc running in neon or argon with admixtures of approximately 10% hydrogen. The arc had a diameter of 4 mm and was operated at currents between 25 and 80 A. To extend the electron density range covered by the experiment the pressure of the arc plasma was varied from 1 to 6 atm. The α as well as the β line of the Paschen series are situated in a wavelength region where the observation is disturbed by absorption of water vapor from the air. While in the case of P_α the whole line profile is influenced, the absorption of the P_β is limited to the red wing. Therefore, the complete setup including the spectrometer was operated under vacuum. In Fig. 1 the response of our detection system is shown for the wavelength range between 0.5 and 3 μm for atmospheric pressure and vacuum. The observed curves represent the combined influence of the emission of the tungsten wire of the lamp used and the spectral response of the detector and the monochromator. The absorption bands can clearly be seen in the spectrum recorded under atmospheric pressure. They are essentially removed in the upper spectrum.

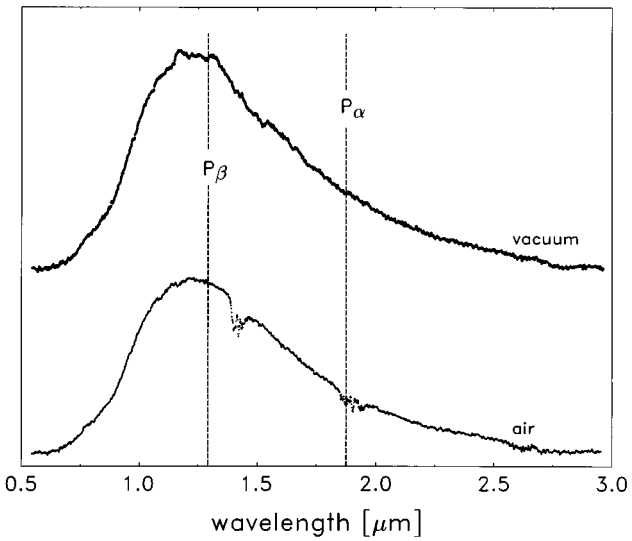

FIG. 1. Spectrum of a tungsten filament at $T=2400$ K recorded for the cases that the experimental setup was operated under atmospheric pressure and vacuum, respectively. The wavelength positions of P_α and P_β are indicated.

A 2 m Czerny-Turner monochromator equipped with a 300 lines/mm plane grating blazed at 1.8 μm was used for the recording of the profiles. A 1.6 μm cut on interference filter suppressed the higher order spectra in the case of P_α. While this setup was favorable for recording the α line the measurements for the β line suffered from the reduced efficiency of the grating and the lower intensity of the line itself. In order to increase the signal to noise ratio, the measurements of P_β at electron densities lower than 2×10^{16} cm^{-3} were additionally performed with a 590 lines/mm plane grating blazed at 1.3 μm. Though in this case the efficiency was better, the slit widths had to be increased in this case in order to obtain a reasonable spectra. Higher order spectra were suppressed by a Schott RG 780 glass filter. The apparatus width was 3.3 Å in the case of P_α and 4 Å in the case of P_β. A 1/3 m monochromator with a Hamamatsu R 928 photomultiplier was used as a monitor for the simultaneous determination of the plasma parameters.

A thermoelectrically cooled lead sulfide element (Infrared Associates, Inc: PS-3) served as a detector in the infrared region and a lock-in technique was used for the amplification

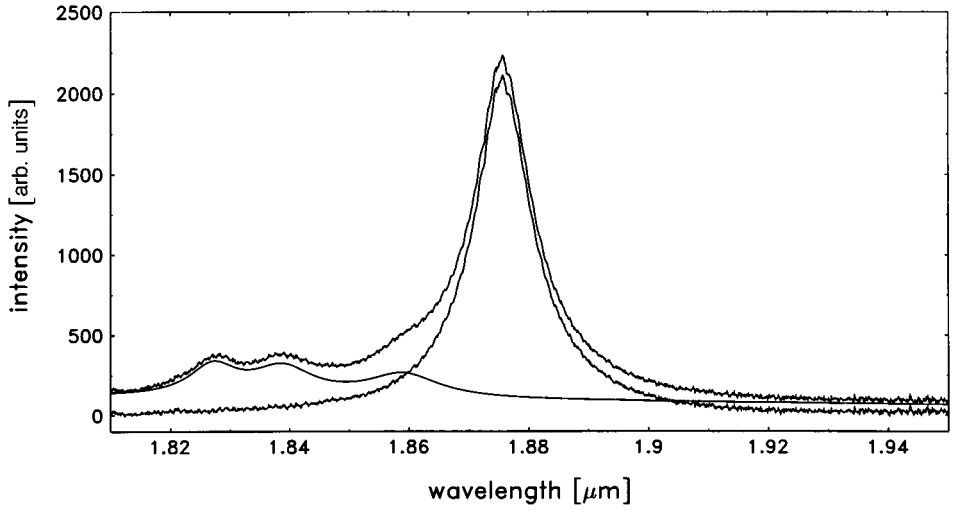

FIG. 2. P_α in neon at an electron density of 6.6×10^{16} cm^{-3}. The spectra show (from top to bottom) the measured data, the result of the fitting procedure for the neon background, and the difference between these two datasets.

of the signal. To avoid problems with a rotating blade chopper in the vacuum system, an electromechanically driven tuning fork device with a resonance frequency of 188 Hz was installed. Since both the lines investigated extend over a wide wavelength region, it was essential to take the spectral response of the detection system into account while analyzing the data. The relative spectral sensitivity of the optical system was determined with a calibrated tungsten strip lamp in order to correct every dataset before being analyzed.

IV. PLASMA DIAGNOSTICS AND DATA REDUCTION

The electron density was determined from the Stark broadening of the Balmer β line. This line was recorded simultaneously with the Paschen lines employing a second monochromator. The half-width of the H_β line and the Stark-effect parameters of [14] were used to calculate the electron density. The estimated uncertainty was 6%. An exact determination of the electron temperature is not necessary for our purpose, because the influence of this quantity on the Stark-effect profile is rather small. In the case of the argon arc one can assume the plasma to be in the state of local thermodynamic equilibrium (LTE). Therefore it is possible to get a reasonably accurate estimate for the temperature from the measured electron density and the plasma calculations [15]. This is more difficult for the neon plasma. Even for the highest electron densities obtained in our measurements LTE is not established [16]. To avoid a nonlocal thermodynamic equilibrium (NLTE) analysis of the neon plasma we used the same method as in the argon case, well aware that the temperatures derived in this way give only a rather rough estimate.

Both the neon and the argon spectra show in the blue wing of P_α several disturbing lines. At relatively small electron densities their influence is rather limited because of their negligible intensity or clear separation from the line core. With increasing electron density both the width of P_α and the intensity of the background lines increase rapidly. This leads to a growing importance of the nearby lines of the carrier gas, causing difficulties in the determination of half-width and position of P_α. Using a least-squares fitting routine [17] the influence of the spectral lines of neon and argon was taken into account (see Fig. 2 and Fig. 3), assuming that the line profiles are of a Voigt shape.

The optical depth of the α line was checked by placing a focusing mirror behind the arc column, thus doubling the effective plasma layer (Fig. 4). Because of the number of free parameters the model function of the fitting routine did not include the optical depth. The Lorentzian half-width L_{fit} given by the least-squares analysis of the recorded spectra of

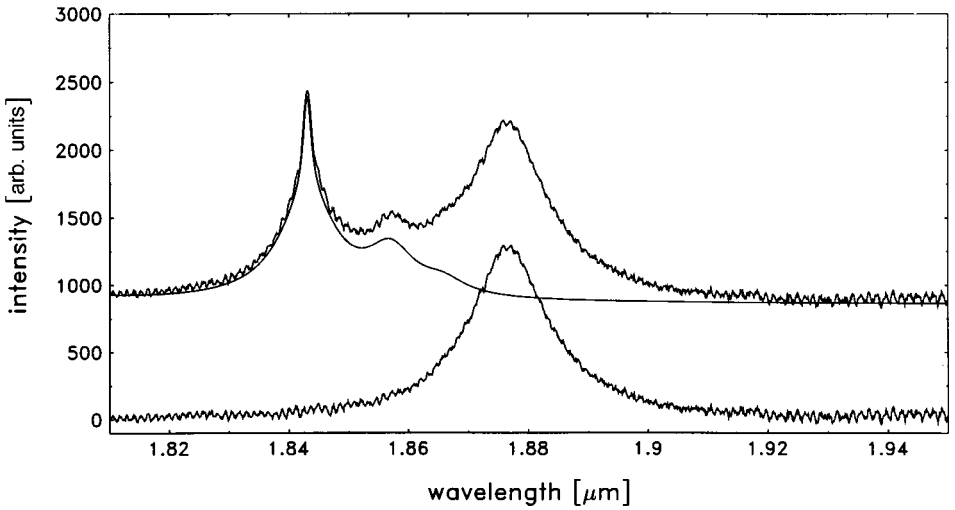

FIG. 3. P_α in argon at an electron density of 14.8×10^{16} cm^{-3}. The order of the data is similar to Fig. 2.

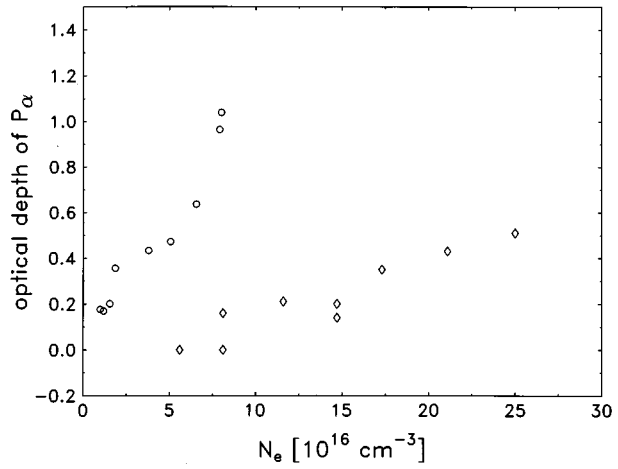

FIG. 4. The optical depth of P_α measured by means of a spherical mirror. Circles and diamonds indicate the use of neon and argon as the carrier gases, respectively.

P_α was corrected using the formula

$$L_{\text{corr}} = L_{\text{fit}}\left(1 - \frac{\tau}{k}\right) \tag{9}$$

with L_{corr} being the corrected Lorentzian half-width. The correction factor is $k=4$ for the Voigt profiles, if two prerequisites are met: the optical depth must not exceed 1 and the Lorentzian width has to dominate the Gaussian width [18]. In our experimental conditions the second of the two prerequisites is always fulfilled: even for the lowest electron densities the ratio of Lorentzian to Gaussian half-width exceeds 4. But the first of the prerequisites is crucial because at electron densities of approximately 8×10^{16} cm^{-3} the optical depth becomes as large as $\tau\approx1$, if the experiment is carried out in neon. For $\tau>1$ the correction factor k decreases. Therefore Eq. (9) would result in corrected widths still being too big.

In the case of P_β no model function to be fitted was available. Nevertheless the background of the carrier gases is crucial. In the case of argon an exact examination of the β line is quite difficult because of neighboring argon lines being more intensive than the hydrogen line itself. Therefore this part of the experiments was carried out mainly in neon. Though this gas shows several lines in the spectral region of P_β, the analysis of the data is hardly disturbed by these profiles, as the half-widths of the neon lines are small compared with the widths of P_β (Fig. 5). Much more important is a broad feature of the neon background. The origin of the feature could not be revealed. It is not related to any series limit of neon. It arises perceptible from the continuum at electron densities above approximately 2×10^{16} cm^{-3} and exhibits a steeper decline to shorter wavelengths than to longer ones. In order to treat the problem we subtracted spectra of pure neon from the spectra of neon with additions of hydrogen recorded at identical electron densities. Because of the smaller transition probability the optical depth of P_β was not as crucial as the optical depth of P_α.

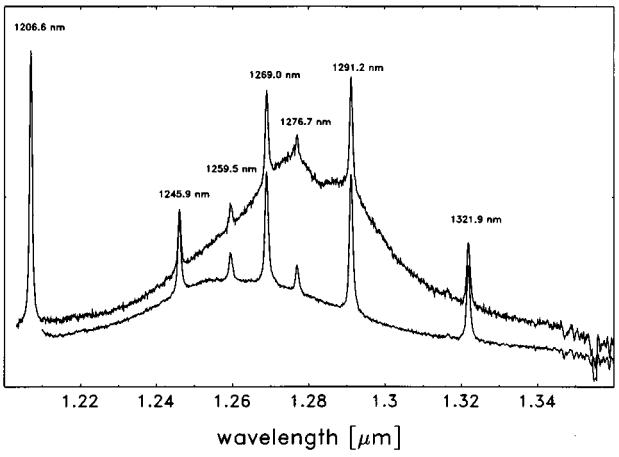

FIG. 5. Spectra of neon with (top) and without (bottom) addition of hydrogen, recorded at an electron density of 9.4×10^{16} cm^{-3} and a pressure of 4 atmospheres. Absorption due to water vapor can be seen in the far red wing of P_β.

TABLE I. Experimental width (FWHM) optical depth τ, and shift $\Delta\lambda$ of P_α in argon. Temperature T according to [15].

N_e [10^{16} cm^{-3}]	p [bar]	T [K]	FWHM [Å]	τ	$\Delta\lambda$ [Å]
5.6	1	11 710	78.8	0	5.9
8.1	1	12 360	104.7	0.16	7.0
11.6	1	13 620	134.5	0.21	10.0
14.7	1	13 870	159.8	0.2	14.4
17.3	1.4	13 900	186.6	0.35	15.5
21.1	2.3	13 380	209.6	0.43	19.2
25.0	3	13 370	242.8	0.51	24.1

In order to determine the shift of the infrared lines an unshifted wavelength marker would have been desirable. Though efforts have been made using various low pressure gas discharges of different design and filling, in all attempts the population of the important levels proved to be too small to observe the lines with an acceptable signal to noise ratio. A reasonable detection of an unshifted P_α or P_β line was neither possible in emission nor in absorption. Thus the unshifted position of the lines was determined by extrapolating the position towards the vanishing electron density. In the case of P_α six data points obtained in neon at electron densities beyond 2×10^{16} cm^{-3} were chosen for this purpose and a linear fit was calculated. In the case of the β line the fitting process included all datapoints.

TABLE II. Experimental width FWHM, optical depth τ, and shift $\Delta\lambda$ of P_α in neon. Temperature T according to [15].

N_e [10^{16}cm^{-3}]	p [bar]	T [K]	FWHM [Å]	τ	$\Delta\lambda$[Å]
0.5	1	12 130	20.9	0.1	1.0
1.0	1	12 990	26.0	0.18	1.1
1.2	1	13 250	30.6	0.17	1.2
1.6	1	13 650	37.1	0.21	1.5
1.9	1	13 910	42.4	0.35	1.8
3.8	1.7	14 630	75.3	0.44	3.4
5.1	2	14 950	97.4	0.48	4.6
6.6	2.6	15 170	121.5	0.63	6.3
7.9	3.6	15 210	153.4	0.96	7.7
8.0	4.4	16 020	160.4	1.04	8.0

TABLE III. Experimental width FWHM of P_β in neon.

N_e [10^{16} cm^{-3}]	FWHM [Å]
0.5	46
0.7	59
1.1	82
1.5	103
2.0	128
3.0	185
3.4	192.8
4.0	224.1
5.4	284
5.9	286.7
7.3	343.9
8.2	354.3
10.1	398.7
11.1	443
12.1	489.9

TABLE IV. Experimental width FWHM of P_β in argon.

N_e [10^{16} cm^{-3}]	FWHM [Å]
1.3	101
1.8	136
2.3	145
3.1	201
3.3	213
6.8	302
9.1	390

V. RESULTS AND DISCUSSION

A. Paschen α

The optical depth of P_α was measured as described earlier. As can be seen in Fig. 4, we obtained optical depths up to the order of one in neon and up to $\tau=0.5$ in argon. The Lorentzian width of P_α as given by the results of the fitting routine was corrected following Eq. (9). The position of the line was determined at the maximum of the fitted Voigt profile. The obtained results for the optical depth, the (corrected) width and the shift of the line at different plasma conditions are shown in Tables I and II for measurements in argon and neon, respectively.

According to the linear Stark effect, the width of P_α shows a dependence on the electron density proportional to $N_e^{2/3}$. In Fig. 6 the measured data are compared with the results of the Green's-function approach, with the theoretical results of Kepple and Griem [19] and a computed result according to the model microfield method by Stehlé [20]. Additionally an experimental width obtained by Hepner [21] is shown.

As seen in Fig. 4, in neon the optical depth of P_α exceeds at the identical electron densities the optical depth of P_α in argon. In neon at an electron density of 8×10^{16} cm^{-3} the optical depth is of the order of 1. Here the application of Eq. (9) reaches its limits. This is the reason for the systematic deviations of the corrected widths obtained in argon and neon at identical electron density. The perpendicular error bars include the uncertainty of the fitting process and of the measured optical depth, but exclude possible additional errors produced by optical depths too large for an application of Eq. (9).

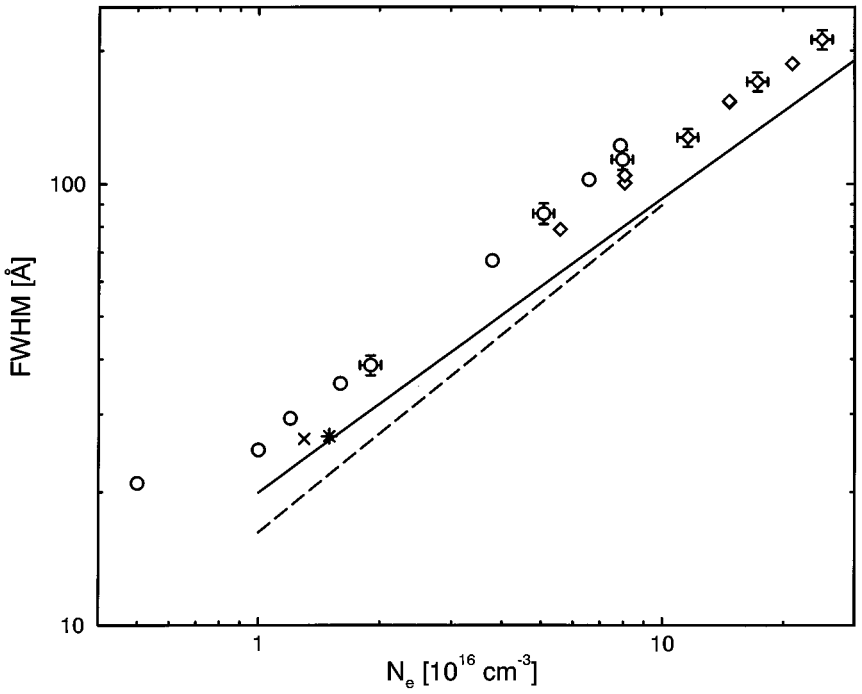

FIG. 6. Full width at half maximum of P_α versus electron density. circle: experiment, neon (this work), diamond: experiment, argon (this work), star: experiment, Hepner [21], cross: theory, Stehlé [20], solid line: theory, this work, dashed line: theory, Kepple and Griem [19].

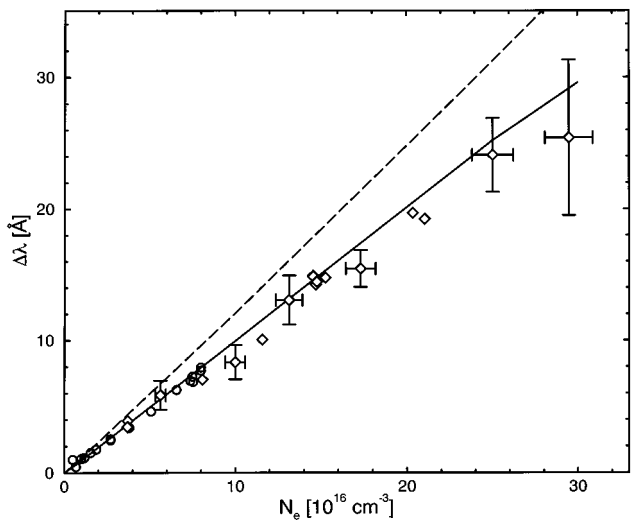

FIG. 7. Maximum shift of P_α versus electron density. circle: experiment, neon; diamond: experiment, argon; dashed line: theory, according to approximations Eqs. (5) and (7); solid line: theory, dynamic screening.

The experimental result of Hepner [21] deviates from our data towards smaller widths, probably because of difficulties in the determination of the electron density in this early work. The theoretical calculations not including ion dynamics [19] produce widths being too small by a factor of approximately 1.3 at an electron density of 10^{16} cm^{-3} and 1.13 at a density of 10^{17} cm^{-3}. Our calculated widths, including ion dynamics, do not fit the experimental data much better, and also tend to be too small. However, these discrepancies between experimental and theoretical half-widths had to be expected. It is well known that the applied model microfield method underestimates the effects due to ion dynamics. The calculated and measured shifts of P_α versus electron density are shown in Fig. 7. The experimentally obtained results agree very well with the calculations including the dynamic screening following the Green's-function approach. With growing electron density deviations from the linear behavior become visible. Therefore one may conclude that a binary collision approximation becomes questionable for densities larger than 10^{17} cm^{-3}. For higher densities the interaction between the radiator and a perturbing electron becomes dynamically screened by the surrounding plasma.

The uncertainty of the determination of the position of P_α increases with the broadening of the neighboring lines of the carrier gas, as the lines overlap more and more. This is especially important in the case of argon (Fig. 3). At an electron density of approximately 3×10^{17} cm^{-3} the error becomes as large as 23%. In spite of that a nonlinear dependence of the shift on the electron density is clearly observed.

B. Paschen β

The half-width of P_β was obtained directly from the measured spectra after subtraction of the neon background and the spectral correction. We used the mean of the blue and red maxima as a definition of the maximal intensity of the line. The experimental and theoretical results are shown in Fig. 8. One recognizes a very good agreement particularly at electron densities exceeding 1×10^{16} cm^{-3}. At lower densities our measured data tend towards smaller widths. A possible explanation is the adverse signal to noise ratio at these densities complicating a proper determination of the depth of the central minimum of P_β. This might lead to a supposed minimum lying too high and therefore causing smaller widths than calculated.

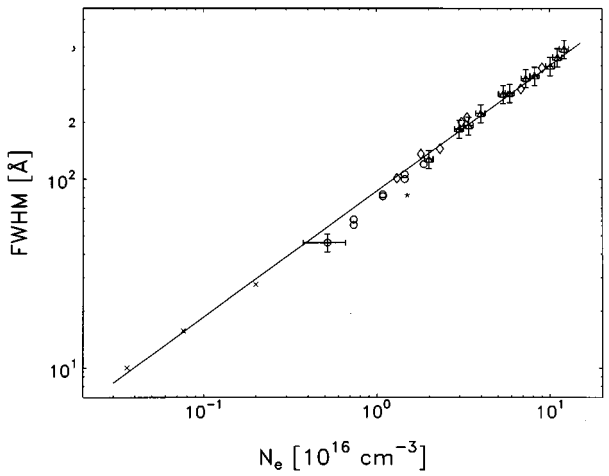

FIG. 8. Full width at half maximum of P_β versus electron density. circle: experiment, neon (this work), diamond: experiment, argon (this work), cross: experiment, Castell *et al.* [22], star: experiment, Hepner [21], solid line: theory, this work.

A comparison with the results of two other experiments is possible. As in the case of P_α the width given by Hepner [21] is smaller than ours. Measurements of Castell *et al.* [22] at electron densities being approximately one order of magnitude smaller than ours agree very well with the theoretical results.

Like the half-width of the line the separation of the maxima of P_β shows a dependence on the electron density proportional to $N_e^{2/3}$ (Fig. 9). According to Fig. 10 the ratio of peak separation and half-width is therefore nearly constant. The mean value of the ratio obtained in our measurements is 0.31 with a statistical uncertainty of 20% because of the signal to noise ratio at low electron densities. (Also see Tables III and IV.)

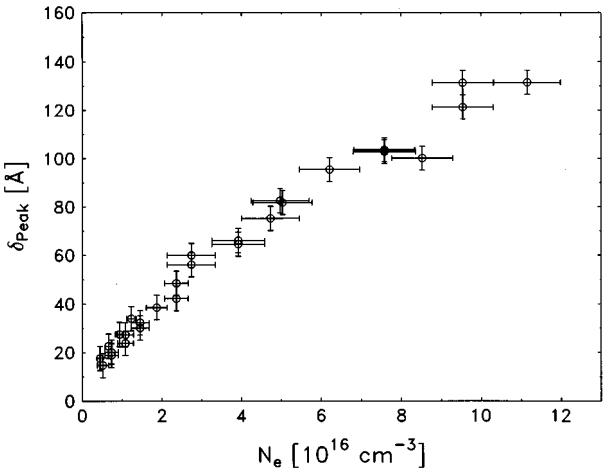

FIG. 9. Separation of the maxima of P_β versus electron density.

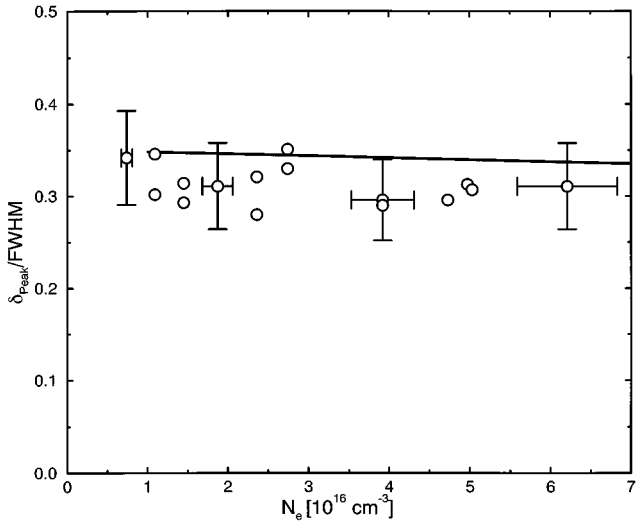

FIG. 10. Ratio of peak separation to full width at half maximum of P_β versus electron density. The full line indicates the theoretical values.

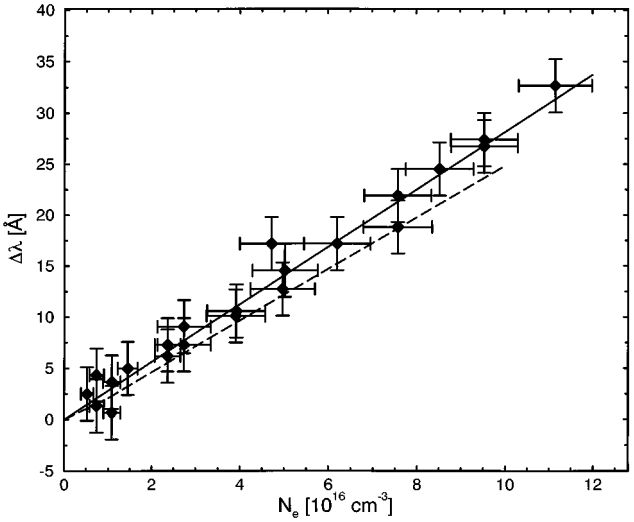

FIG. 11. Dip shift of P_β versus electron density. The dashed line indicates the calculated shift, the solid line a linear fit through the experimental data.

To determine the position of the line we choose to take the position of the central minimum. The advantage of this dip-shift method is a smaller dependence on the structure of the neon background, thus giving more reliable results when compared to methods taking the position of the line at a fraction of the maximum intensity, for example. Figure 11 shows the data of this work. Both theoretically predicted and experimentally observed shifts of P_β behave linearly, though the first ones tend to smaller shifts than measured. A linear fit to the experimental results gives a shift of 28 Å at an electron density of 1×10^{17} cm^{-3}, whereas the corresponding theoretical shift is about 25 Å.

ACKNOWLEDGMENTS

This work was partly funded by the Deutsche Forschungsgemeinschaft (He 876/10) and by the Sonderforschungsbereich 198.

[1] D. E. Kelleher, W. L. Wiese, V. Helbig, R. L. Greene, and D. H. Oza, Phys. Scr. **T47**, 75 (1993).
[2] V. Helbig, Contrib. Plasma Phys. **31**, 183 (1991).
[3] G. Röpke and R. Der, Phys. Status Solidi B **92**, 501 (1979).
[4] L. Hizschke, G. Röpke, T. Seifert, and R. Zimmermann, J. Phys. B **19**, 2443 (1986).
[5] S. Günter, L. Hitzschke, and G. Röpke, Phys. Rev. A **44**, 6834 (1991).
[6] S. Günter, Phys. Rev. E **48**, 500 (1993).
[7] A. Brissaud, C. Goldbach, L. Leorat, and A. Mazure, J. Phys. B **9**, 1147 (1976).
[8] J. Seidel, Z. Naturforsch. Teil A **32**, 1195 (1977).
[9] J. Seidel, Z. Naturforsch. Teil A **35**, 679 (1980).
[10] A. Brissaud, C. Goldbach, J. Leorat, A. Mazure, and G. Nollez, J. Phys. B **9**, 1129 (1976).
[11] J. Halenka, Z. Phys. D **16**, 1 (1990).
[12] L. Kudrin and G. Sholin, Dokl. Akad. Nauk SSR **147**, 342 (1963) [Sov. Phys. Dokl. **7**, 1015 (1963)].
[13] G. Sholin, Opt. Spectrosc. **26**, 275 (1969).
[14] V. Helbig and K.-P. Nick, J. Phys. B **14**, 3573 (1981).
[15] J. Irmer and M. Worm, *Die Zusammensetzung Thermischer Edelgasplasmen* (Akademie-Verlag, Berlin, 1974).
[16] J. Uhlenbusch, E. Fischer, and J. Hackmann, Z. Phys. **239**, 120 (1970).
[17] K. Jeβ, V. Helbig, F. Greiner, J. Kaspareit, V. Rohde, and T. Weirauch, J. Quant. Spectrosc. Radiat. Transfer **41**, 69 (1989).
[18] F. Greiner (unpublished).
[19] P. C. Kepple and H. R. Griem, Phys. Rev. **173**, 317 (1968), and private communication.
[20] C. Stehlé (private communication).
[21] G. Hepner, C.R. Acad. Sci. **241**, 380 (1955).
[22] R. Castell, D. Mandelbaum, A. Mendez, and A. Sanchez, J. Quant. Spectrosc. Radiat. Transfer **30**, 345 (1983).